Insights of Electrical Engineering and Technology
https://ojs.achpub.com/IEET

Communication

Highly Isolated Dual Circularly Polarized Metallic ME-dipole Antenna Array Design

Oludayo Sokunbi *, Ahmed A. Kishk

Department of Electrical and Computer Engineering, Concordia University, Montreal, QC H3G 1M8, Canada
* Correspondence: sokunbidayo@gmail.com

Received: 17 June 2025; **Revised:** 10 July 2025; **Accepted:** 21 July 2025

Abstract: A novel dual circularly polarized metallic magneto-electric dipole (D-CP-M-ME-dipole) for the 30 GHz band is presented. The D-CP-M-ME-dipole uses solid metallic aluminum bulk without surrounding it with metallic cavities. It is fed by crossed narrow slots coupled to air-filled microstrip lines packaged by a bed of printed periodic mushrooms, achieving a bandwidth of 26–41 GHz (46%). An 8×8 array is constructed and fed by a carefully designed dual-polarized cooperative feeding network, which is optimized considering the mutual coupling influence. Hence, the need for an external decoupling mechanism to isolate the two polarizations is eliminated. The feed network is on Printed gap waveguide (PGW) to prevent leakage. Furthermore, parasitic elements are added to the 8×8 array to realize a 9×9 element array that improves the overall gain over the bandwidth. The 9×9 dual CP metallic ME- dipole is fabricated and measured to verify this procedure, with an ultrawide impedance bandwidth of 26–42 GHz (47%), 26.6 dBic gain, and 90% total efficiency, with less than 40 dBi isolation between the two polarizations throughout the band.

Keywords: magneto-electric dipole; microstrip ridge gap waveguide (MRGW); circular polarization; antenna arrays

1. Introduction

Dual circularly polarized antennas have been recently discussed in the literature because they can reduce polarization mismatches, mitigate multipath propagation, enhance better mobility, and reduce other interference by exciting two orthogonal *E* vectors, Right-Hand Circular Polarization (RHCP) and Left-Hand Circular Polarization (LHCP) that are equal in amplitude and in-phase quadrature (±90°) [1]. Hence, they are good candidates for satellite navigation, aerospace, radar, and mobile portable communication systems because they can overcome limitations associated with linear polarizations [2]. The 3-dB Axial Ratio (AR) bandwidth of CP antennas is usually more than 15% to meet this requirement. Therefore, most CP arrays usually require a sequential rotation feed network to meet this requirement. CP can be generated in antennas in different ways, and they are broadly categorized into single and multi-probe feed systems, depending on the bandwidth requirement. In [3], a 4-layer *k*-band 8×8 dual-circularly polarized antenna was presented. Two stacked chamfered square patches and two orthogonal slots are utilized to realize dual circular polarization around 18.8–20 GHz, with less than 15 dB polarization isolation and 75% aperture efficiency. The sequential rotation feed network technique is employed to achieve a dual circularly polarized antenna on a single layer between 27–33 GHz bandwidth, with less than 20 dB isolation and 11.8 dBi gain [4]. The authors in [5] utilized two suspended metal posts, and two semi-circular patches with orthogonal slots to achieve dual-CP in a 4-layer 4×4 patch antenna around 26–35 GHz with a peak gain of 14.5 dBi. In [6], left-hand CP (LHCP) and right-hand CP (RHCP) are achieved in the 20 and 30 GHz bands, respectively, in a 3-layer,

DOI: https://doi.org/10.64897/ieet.2025v1i1.001

2×2 array using printed ridge gap waveguide (PRGWG) and stacked patches, with 19.4-20.4 and 28.5-31.4 GHz AR bandwidths with 13.2 and 11.5 dBci gain, respectively. Dynamic and Berry phase compensation techniques are explored to realize a low-profile 2×2 dual-CP antenna, with 28 dBci maximum gain and 27–36 GHz AR bandwidth [7]. In [8], a 4-layer sequentially rotated 90° 2×2 array with a feed network is employed to realize 57–72.3 GHz (23.8%) 3dB AR and impedance bandwidth, with 20.5dBci maximum gain. In [9], a dual-band polarized CP antenna was presented by reusing the feed network of the ME-dipole as a radiating slot antenna. The patches form the LHCP, while the microstrip line and slot form the RHCP. A polarization converter is employed in [10] to convert a four-port linear polarization (LP) MIMO antenna to CP at upper and lower bandwidths of 29.25–30.35 and 19.65–22.05 GHz, respectively. The authors in [11] also utilized a polarization-twisting metasurface that converts LP to dual-band (12.25–12.95 GHz and 14.00–14.55 GHz) dual-CP in the Ku-band. The polarization-twisting metasurface consists of a dual-linear-to-circular polarization converter (DLCPC) and a linear polarization conversion metasurface (LPCM). A partially reflective surface (PRS) is added to a dual LP feed network to realize dual-CP radiation [12]. A partially reflecting metasurface is integrated into a Fabry-Perot (FP) antenna to split LP waves into RHCP and LHCP [13]. In [14], varactor diodes are employed to switch the operation band of a patch antenna, while a feed network loaded with pin diodes is employed to convert the LP to LHCP and RHCP. The antenna can achieve continuous frequency adjustment from 2–2.7 GHz with LHCP and RHCP. A dual-polarized filtering antenna is used to illuminate a dielectric lens, consisting of a CP polarizer and phase shifters, capable of converting LP waves to dual-CP waves around 60 GHz [15]. Other filtering antennas have also been recorded where either a bandpass filter is cascaded to a CP antenna [16, 17] or integrating a CP radiator to resonators [18, 19]. In another approach, a filtering power divider network excites two orthogonal modes to achieve CP [20–25].

Millimeter (mmwave) wave frequency bands have advanced features of high capacity, fast data rate, and large bandwidth. However, they are subject to atmospheric losses, especially for long-range communication. Hence, high-gain antennas are in high demand to compensate for the propagation losses [26]. The guiding structures of high-gain mmwave antennas must be properly designed to mitigate spurious radiations [27–32]. Many guiding structures, including Substrate Integrated Waveguide (SIW) [33] and gap waveguide technology [34], can be used in mm-wave antennas.

Here, an 8×8 dual circularly polarized metallic magneto-electric dipole (D-CP-M-ME-dipole) fed by microstrip printed gap waveguide technology is presented. The D-CP-M-ME-dipole antenna element consists of 4 metallic pins and a crossed slot. To obtain dual circular polarization (LHCP and RHCP), a diagonal metallic strip is inserted at the opposite corners of the metallic pins to convert the linear polarizations from the crossed slots to two orthogonal linear modes with (90°) phase shifts by perturbing the waves. Unlike other work where several layers or feedings are the source of CP, the ME-dipole design is the source of the RHCP and LHCP. The 3dB axial ratio and −10 dB impedance bandwidth overlap between 26–42 GHz (47%). The corporate feed network is constructed by extrapolating the mutual admittance matrix of a large array (8×8) from a small array (4×4). The frequency-dependent effective impedance of the large array is then extracted from the small array by considering the mutual coupling effect.

This work extends the idea in [35] by designing a single-layer dual circularly polarized feed network using the frequency-dependent effective impedance termination, unlike other dual-polarized feeding networks that use multi-layers for polarizations. Also, compared to other ME-dipole elements, this work uses an air-filled ME-dipole without a dielectric material to increase the antenna's efficiency by reducing the losses. Compared to other air-filled ME-dipoles [36–39], this work has no cavity but with a high impedance bandwidth. Therefore, the contributions in this work are:

1. Enhancing the single-linearly polarized array architecture presented in [35] by extending it to support dual circular polarization (CP), incorporating frequency-dependent behavior to improve performance across a broader spectrum.

2. Developing a compact, air-filled dual-polarized ME-dipole antenna that eliminates the need for a surrounding open cavity wall, as required in previous designs [36–39]. This design significantly reduces structural complexity while achieving a wide bandwidth of 46% with high radiation efficiency.

3. In large arrays exceeding 4×4 elements, single-layer feeding networks introduce increased spacing between adjacent 4×4 subarrays compared to inter-element gaps, disrupting the aperture's power distribution and reducing gain and efficiency. To address this, parasitic elements are strategically placed within these inter-subarray gaps. These elements are excited parasitically by surrounding active elements that reradiate in-phase, effectively restoring aperture continuity and significantly improving overall gain and efficiency.

2. Design Mechanism

2.1 *Unit Cell Design*

First, the stop band of the periodic structure must be designed to achieve a stop band that is usually around 1:2 of the frequency band [40]. The printed periodic structure is chosen to be of mushrooms with a unit cell of $L_2 \times L_2$ cross-section as shown in Figure 1. It is composed of a 0.3 mm diameter and 0.508 mm length metallic via connecting the ground on the bottom and a square patch of $L_1 \times L_1$ on the top sandwiching a Rogers RT 6002 substrate of dielectric constant 2.94, loss tangent 0.0012. On top of the square patch, the RT 5880 dielectric constant substrate is 2.2, the loss tangent is 0.0009, and the thickness is 0.254 mm, where the line should be printed. An air gap of height of 0.27 mm separates the last substrate from the upper conductor. The air gap and the top substrate must have an equivalent thickness of much less than a quarter of a wavelength at the upper frequency. A 25–50 GHz stop band is created to suppress any wave from propagating between the mushroom surface and the upper conductor. After that, the microstrip line is inserted to allow the signal to propagate between the top of the line and the upper conductor. The signal is confined following the line direction. These results are omitted for brevity.

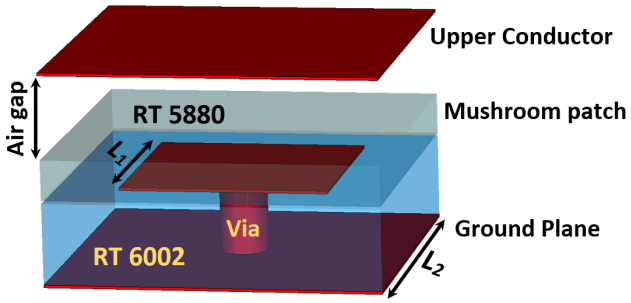

Figure 1. Unit Cell design (L_1= 0.79 mm, L_2= 1 mm).

2.2 *Dual Circularly Polarized Metallic ME-dipole*

The linearly-polarized ME-dipole in [41], which is coupled to the lines through a slot, is modified to achieve a dual-circularly-polarized metallic magnetoelectric dipole (D-CP-M-ME-dipole). A metallic strip is inserted diagonally at the opposite corners of the metallic pins to convert the linear polarizations from the crossed slots to two orthogonal linear modes with 90° phase shifts by perturbing the waves, hence, generating Left and Right-hand circular polarized waves. The D-CP-M-ME-dipole requires 17×17 mushroom cells. To ensure minimum coupling and to improve matching, two orthogonal stub lines are etched at the tips of both transmission lines so that they can excite two distinct polarizations via the air gap. Each feedline is 9 mm long and 0.7 mm wide, carefully placed towards the end of the crossed slots. The crossed slots have dimensions of 0.5 mm × 6 mm. The D-CP-M-ME-dipole is sitting directly on the metallic plate, as shown in Figure 2a, and it consists of 4 pins, each of dimensions 2 mm × 2 mm × 1.5 mm. To generate dual circular polarization, a metallic strip of dimensions 2.1 mm × 0.42 mm is diagonally placed across two adjacent pins to convert the LP coming from the slots to two distinct polarizations of equal magnitude and 90° phase difference (*i.e.*, LHCP and RHCP).

The relative positions of the orthogonal lines with respect to the slot are shown in Figure 2b. The two feedlines are placed around 0.5 mm from the edges of the orthogonal slots. It also shows a clear view of the metallic dipoles and the metallic strip line, which is the source of the circular polarization. Unlike other works where the source of polarization is external to the antenna, it makes the antenna complex. This work has the source of polarization as part of the antenna system itself. Besides, the feed lines generate different modes on the same layer, ensuring compactness and flexibility. The antenna has a total dimension of 17.6 mm × 17.6 mm.

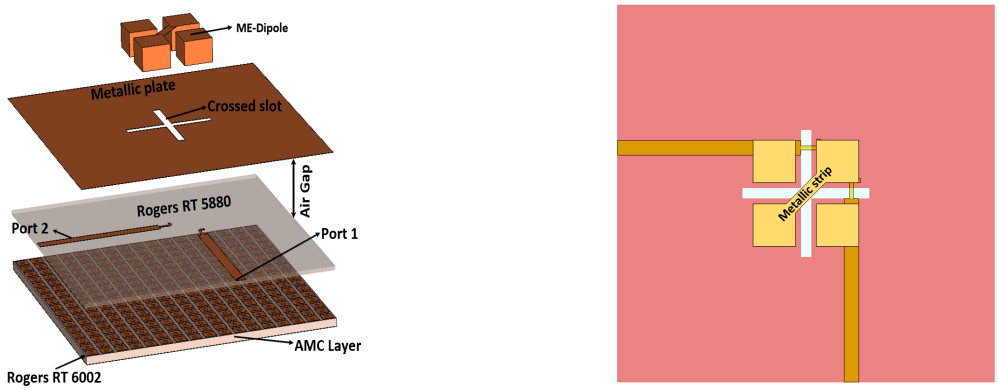

Figure 2. Dual circularly polarized Metallic ME-dipole: (a) 3D Schematic and (b) Top view with a transparency of the conductor sheet to show the lines.

The dual-polarized CP single-element antenna exhibits a 25–41 GHz bandwidth of −10 dB matching, less than 3 dB axial ratio, and isolation better than 40 dB, as shown in Figure 3a,b. Such high isolation results from carefully designing open-circuit stubs at the tip of the feedlines. The antenna has a peak gain of 11.7 dBic, as shown in Figure 4 for both polarizations. The far-field radiation pattern of the single-element antenna at 28, 32, and 38 GHz in the *xz*- and *yz*-planes is shown in Figure 5. The cross-polarization is less than 40 dB at all frequency bands and, hence, not shown.

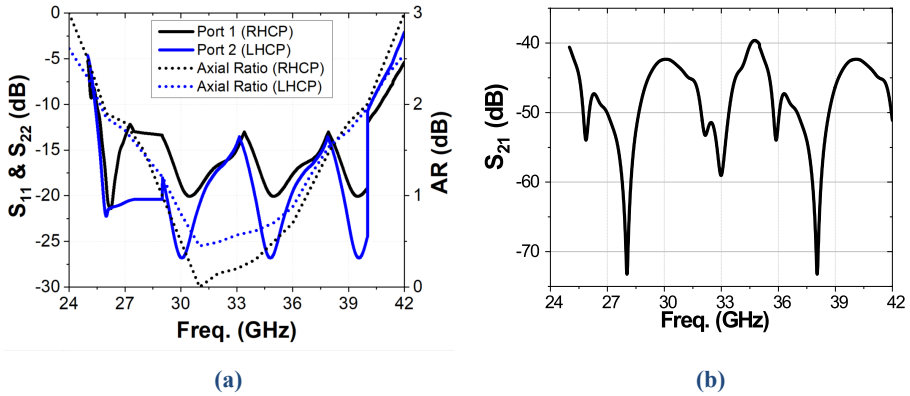

Figure 3. (a) Reflection coefficients and Axial Ratio of the RHCP and LHCP ports and (b) S_{21}, indicating isolation better than 40 dB.

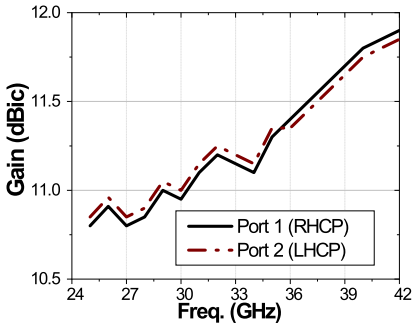

Figure 4. Gain of the dual circularly polarized metallic ME-dipole element.

The far-field radiation pattern of the single-element antenna at 28, 32, and 38 GHz in the *xz* and *yz* planes is shown in Figure 5. The cross-polarization is less than 40 dBic at all frequency bands and, hence, ignored.

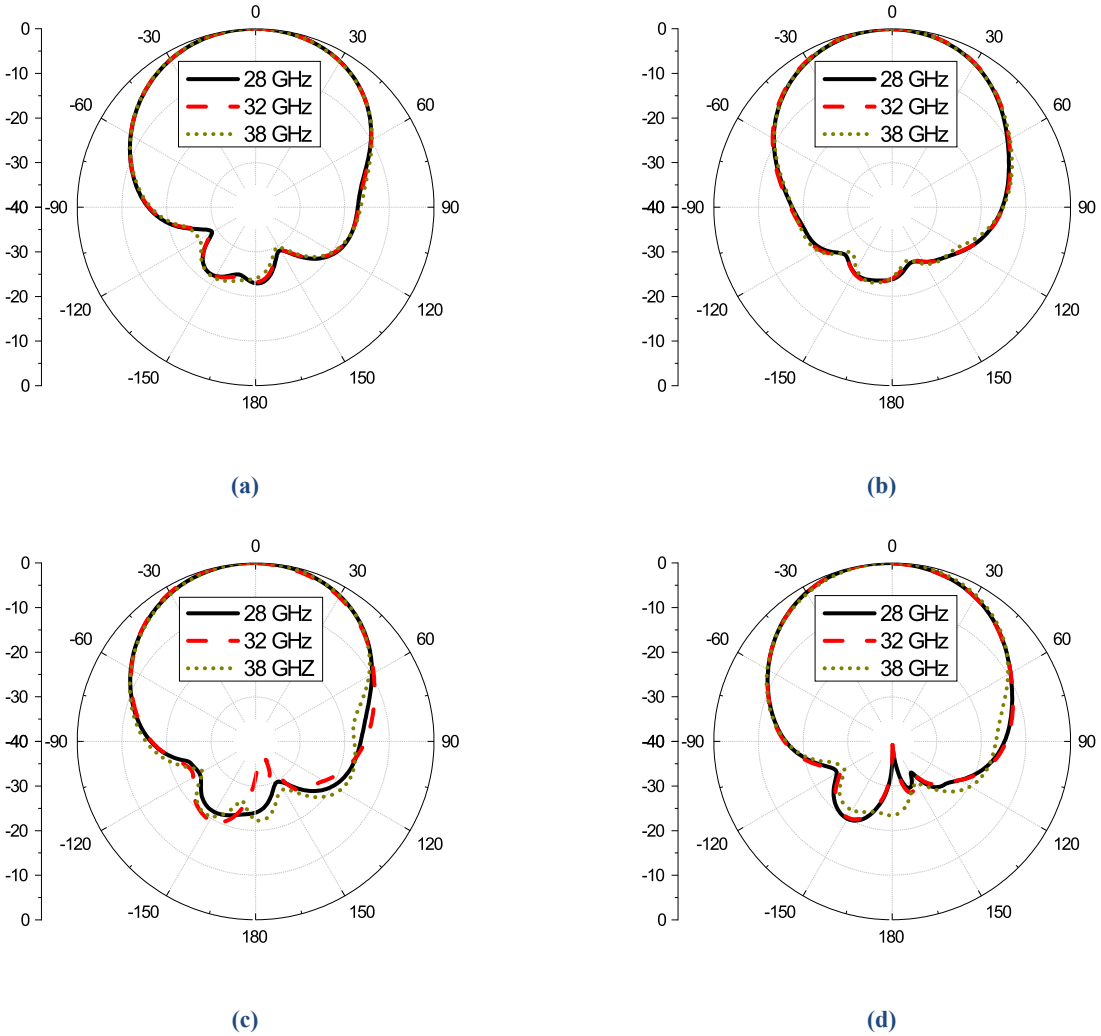

Figure 5. Far-field radiation patterns of the D-CP-M-ME-dipole element: Top for RHCP and bottom for LHCP. Right side *xz*-plane and left side *yz*-plane.

2.3 *8×8 Element CP Array Design*

To design an 8×8 element array, the 4×4 array element of the ME-dipole is first designed without the feeding network to extract the admittance matrix and frequency-dependent input impedance of each element. As a single-layer feeding network is proposed for the two dual-polarized arrays, overlapping and crossovers of the line should be avoided. The element-to-element distances between the elements are d_x and d_y. The fielding network is designed for the 8×8 array as shown in Figure 6. It can be seen that it requires a distance D_x and D_y between 4×4 subarrays' edge elements. Therefore, the ME-dipoles must be placed as shown in Figure 7.

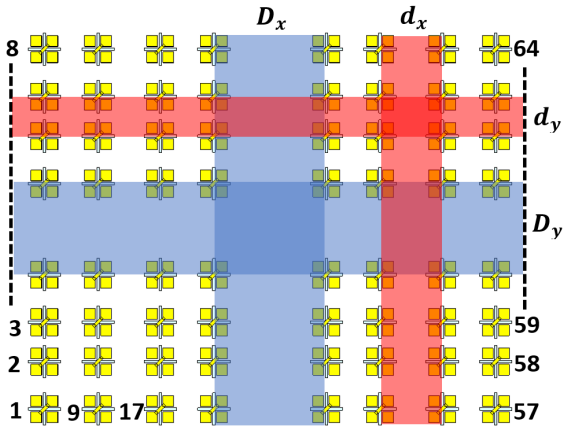

Figure 6. Element arrangements and numbering of the 8×8 array ($d_x = d_y = 0.83$ mm, $D_x = D_y = 1.54$ mm).

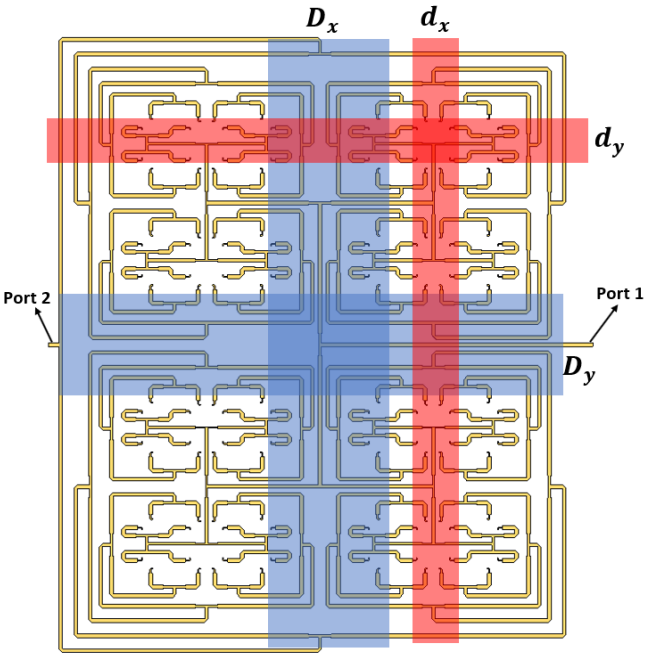

Figure 7. Constructed feeding network of the 8 × 8 array.

To cater for the empty spaces in Figure 6, parasitic elements are added to the active 8 × 8 array, as shown in Figure 8. They are parasitically coupled and act as secondary sources. Their presence improves the array power distribution. Therefore, they enhance the antenna gain. These elements are loaded with slots similar to the active elements. The fabricated array is shown in Figure 9.

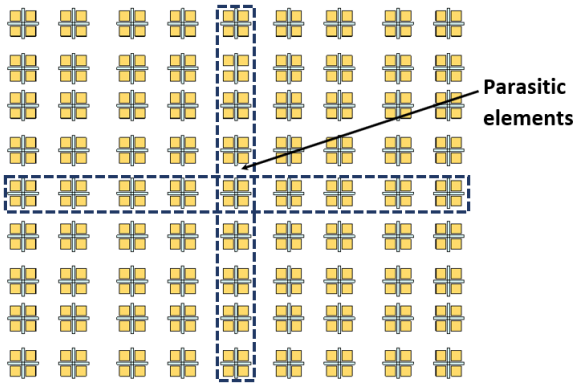

Figure 8. Feed network design of the 8 × 8 active and added parasitic elements.

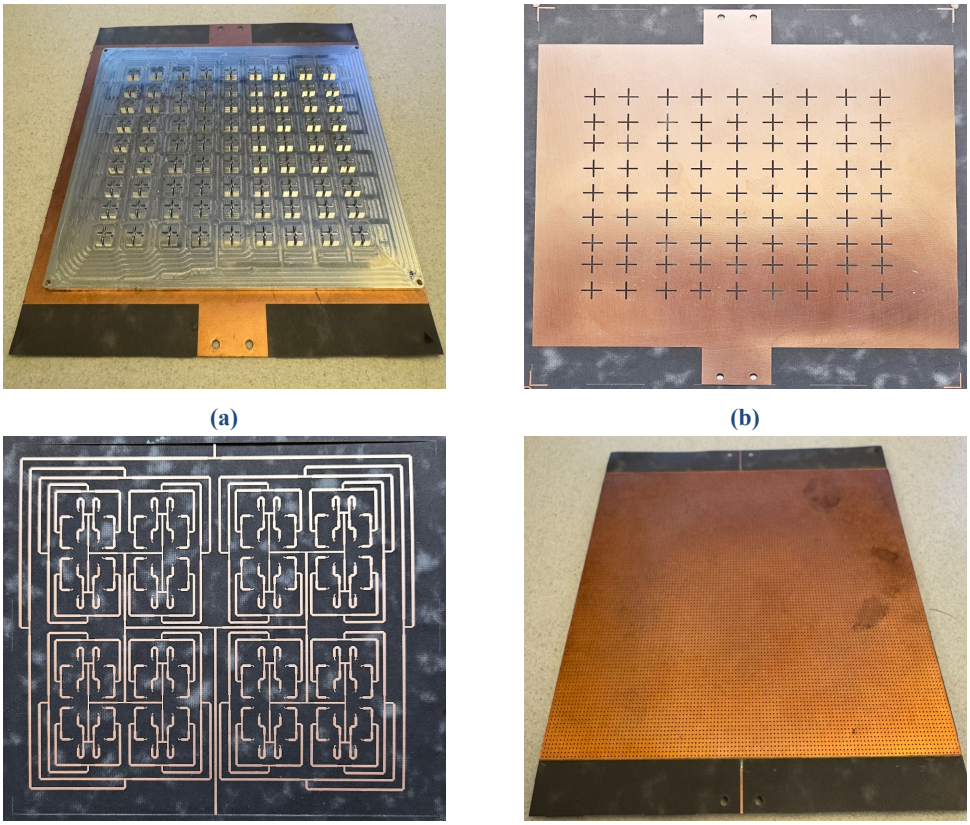

Figure 9. Fabricated prototype of the 9×9 Array: (a) Top layer, (b) slot layer, (c) Feeding network, and (d) AMC layer.

Figure 10 shows the simulated and measured reflection coefficient of the 9×9 array for both RHCP and LHCP. When the simulated results are for the whole structure, including the radiating elements, it is called full-wave. When the feeding network is terminated by the frequency-dependent effective impedances that replace the radiating elements, it is called Eff. Imp. ter.

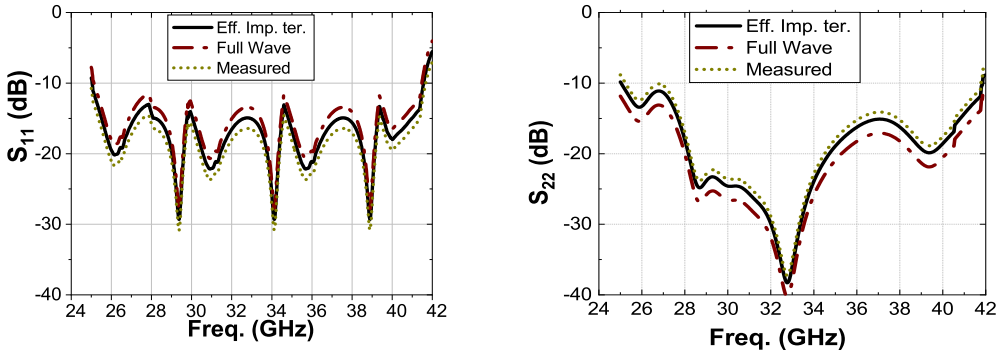

Figure 10. Measured and simulated Reflection coefficients of the 9 × 9 dual CP metallic ME-dipole array (a) RHCP and (b) LHCP.

The simulated and measured AR bandwidths for both polarizations are shown in Figure 11. The AR bandwidth is 24–42 GHz (56%), covering the anticipated impedance bandwidth.

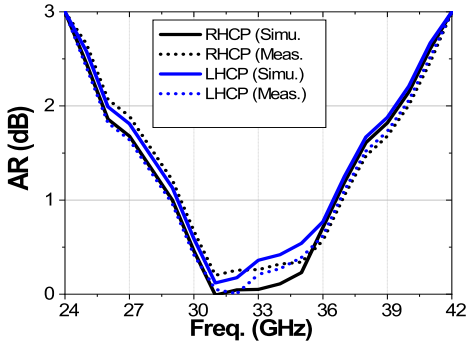

Figure 11. Simulated and measured AR of the 9 × 9 dual CP metallic ME-dipole array.

The simulated and measured polarization isolation using radiation elements or impedance terminations is shown in Figure 12. The isolation is less than 40 dB throughout. This high isolation is attributed to the carefully designed feeding network, which accounts for the mutual coupling between the antenna elements and ports.

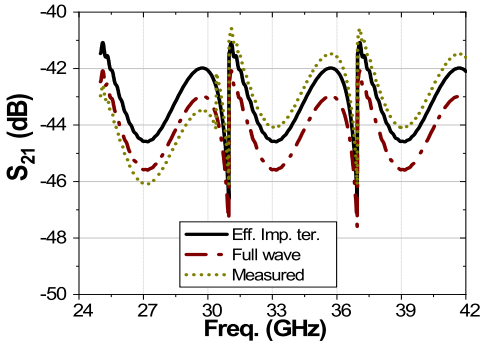

Figure 12. Simulated and measured Isolation between the RHCP and LHCP ports of the 9 × 9 array.

The array gain is simulated with and without the parasitic elements. The measured gain with the parasitic elements is compared with the simulated gain. The parasitic elements have increased the overall gain of the array by an average of 0.2 dB. The *S*-parameters and radiation pattern are unaffacted by adding these parasitic elements. The corresponding simulated and measured total efficiency is also shown in Figure 13. The antenna exhibits a maximum efficiency of 89%.

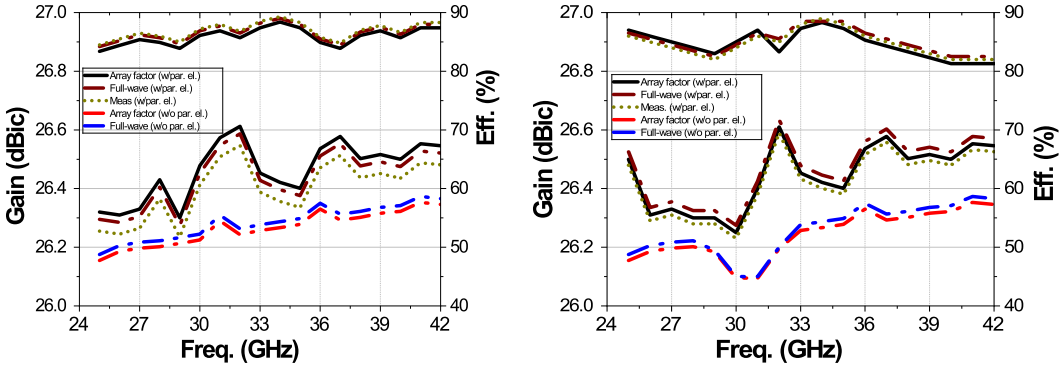

(a) (b)

Figure 13. Simulated and measured gain and efficiency of the Array (a) RHCP (b) LHCP.

The simulated and measured far-field radiation pattern of the 9×9 array at 34 GHz is shown in Figure 14, comparing the array factor method with full-wave simulation. The cross-polarization patterns are less than 40 dB. Therefore, the cross-polarization patterns are not shown. The patterns in the *xz* and *yz* planes look almost the same.

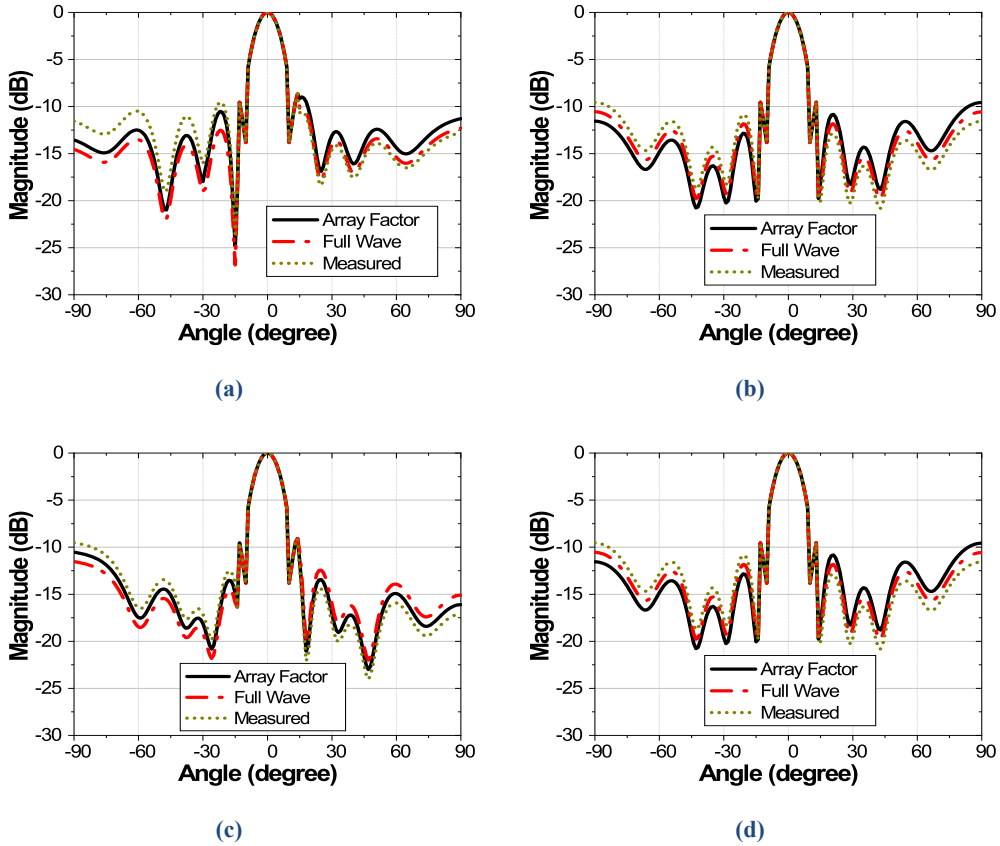

(a) (b)

(c) (d)

Figure 14. Normalized radiation patterns of the array at 34 GHz: Top for RHCP and bottom for LHCP. Right side *xz*-plane and left side *yz*-plane.

It is essential to note that PGW can be lossy when constructing a large antenna array with mushroom AMC. Furthermore, at mm-wave frequencies, mechanical tolerances may be crucial; as a result, additional research may be conducted using empirical equations. The technique of small-to-large arrays can be extended to model arbitrary distributed arrays. This extension can be implemented using machine learning on the small array to generate an arbitrarily distributed small array from which an arbitrarily distributed large array can be efficiently designed. The scanning array can also be studied to test the possible scanning range.

Table 1 compares this work to the recent state-of-the-art. This work shows the highest isolation, bandwidth, and peak gain with just two layers.

Table 1. Comparison with other dual-polarized CP arrays in the literature

Ref.	No. of Elements	Isolation (dB)	No. of Pol.	BW (%)	No. of Layers	Peak Gain (dBic)	Efficiency (%)
[42]	8×8	14	Dual-CP	23/23	6	25.8/25.7	80/80
[43]	4×4	15	Dual-CP	17/17	5	20.8/21.0	90/95
[44]	16×16	13	Dual-CP	16/16	8	32.8/32.8	90/90
Prop.	8×8	40	Dual-CP	47/47	2	26.61/26.62	89/90

3. Conclusion

A dual circularly polarized novel metallic ME-dipole antenna with high isolation has been presented. A diagonal metallic strip line converts the dual LP to dual CP. Compared to other ME-dipole antennae, this work has no dielectric substrate to improve efficiency. The concept of frequency-dependent input impedance has been used to construct the feed network of the 9×9 array by considering the isolation. The 9×9 array exhibits a measured 26.6 dBi peak gain and 90% total efficiency within the 26–41 GHz (47%) bandwidth for both left and right-hand circular polarizations, with less than 40 dB isolation between the two polarizations.

Confilict of Interest

The authors declare no conflict of interests.

References

[1] Toh BY, Cahill R, Fusco VF. Understanding and measuring circular polarization. *IEEE Trans. Educ.* 2003, 46(3): 313–318. [CrossRef]

[2] Rad M, Nikkhah N, Zakeri B, *et al.* Wideband Dielectric Resonator Antenna With Dual Circular Polarization. *IEEE Trans. Antennas Propag.* 2022, 70(1): 714–719. [CrossRef]

[3] Lu S, Qu SW. Dual-Circularly Polarized Phased Array With Modified Cavity and Notched Patch. *IEEE Antennas Wireless Propag. Lett.* 2024, 23(4): 1266–1270. [CrossRef]

[4] Yang YH, Sun BH, Guo JL. A Low-Cost, Single-Layer, Dual Circularly Polarized Antenna for Millimeter-Wave Applications. *IEEE Antennas Wireless Propag. Lett.* 2019, 18(4): 651–655. [CrossRef]

[5] Cheng Y, Dong Y. Dual Circularly Polarized Broadband Antenna Array for Millimeter-Wave Applications. *IEEE Antennas Wireless Propag. Lett.* 2022, 21(12): 2377–2381. [CrossRef]

[6] Liu Y, Yue Z, Jia Y, *et al.* Dual-Band Dual-Circularly Polarized Antenna Array With Printed Ridge Gap Waveguide. *IEEE Trans. Antennas Propag.* 2021, 69(8): 5118–5123. [CrossRef]

[7] Jiang ZH, Yue T, Hong W. Low-Profile and Wideband Dual-Circularly Polarized Reflect-Arrays Based on Rotated Metal-Backed Dual-Polarized Aperture-Coupled Patch Elements. *IEEE Trans. Antennas Propag.* 2020, 68(3): 2108–2117. [CrossRef]
[8] Qi Z, Zhu Y, Li X. Compact Wideband Circularly Polarized Patch Antenna Array Using Self-Sequential Rotation Technology. *IEEE Antennas Wireless Propag. Lett.* 2022, 21(4): 700–704. [CrossRef]
[9] An N, Zhang Y. Dual-Band Dual-Sense Circularly Polarized Antenna Utilizing a Radiating Slot Antenna as Feeding Structure. *IEEE Antennas Wireless Propag. Lett.* 2024, 23(4): 1321–1325. [CrossRef]
[10] Sofi MA, Saurav K, Koul SK. Four-Port Orthogonal Circularly Polarized Dual-Band MIMO Antenna With Polarization and Spatial Diversity Using a Dual-Band Linear-to-Circular Polarization Converter. *IEEE Trans. Antennas Propag.* 2022, 70(9): 8554–8559. [CrossRef]
[11] Yang P, Dang R, Li L. Dual-Linear-to-Circular Polarization Converter Based Polarization-Twisting Metasurface Antenna for Generating Dual Band Dual Circularly Polarized Radiation in Ku-Band. *IEEE Trans. Antennas Propag.* 2022, 70(10): 9877–9881. [CrossRef]
[12] Orr R, Goussetis G, Fusco V. Design Method for Circularly Polarized Fabry-Perot Cavity Antennas. *IEEE Trans. Antennas Propag.* 2014, 62(1): 19–26. [CrossRef]
[13] Yang P, Yang R, Li Y. Dual Circularly Polarized Split Beam Generation by a Metasurface Sandwich-Based Fabry-Pérot Resonator Antenna in Ku-Band. *IEEE Antennas Wireless Propag. Lett.* 2021, 20(6): 933–937. [CrossRef]
[14] Yu Y, Sun M, Zhang Z, *et al.* A Tunable Dual-Circularly Polarized Antenna With Broadband Triple-Branched Feed Structure. *IEEE Antennas Wireless Propag. Lett.* 2022, 21(10): 1965–1969. [CrossRef]
[15] Hu HT, Chan KF, Chan CH. High-Gain Dual-Circular-Polarized Filtering Lens Antenna for Low-Cost 60 GHz Applications. *IEEE Antennas Wireless Propag. Lett.* 2024, 23(2): 828–832. [CrossRef]
[16] Jiang ZH, Gregory MD, Werner DH. Design and Experimental Investigation of a Compact Circularly Polarized Integrated Filtering Antenna for Wearable Biotelemetric Devices. *IEEE Trans. Biomed. Circuits Syst.* 2016, 10(2): 328–338. [CrossRef]
[17] Sahoo AK, Gupta RD, Parihar MS. Circularly polarised filtering dielectric resonator antenna for X-band applications. *IET Microw. Antennas Propag.* 2018, 12(9): 1514–1518. [CrossRef]
[18] Dong Y, Gao S, Luo Q, *et al.* Broadband Circularly Polarized Filtering Antennas. *IEEE Access*. 2018, 6: 76302–76312. [CrossRef]
[19] Li T, Gong X. Vertical Integration of High-Q Filter With Circularly Polarized Patch Antenna With Enhanced Impedance-Axial Ratio Bandwidth. *IEEE Trans. Microw. Theory Tech.* 2018, 66(6): 3119–3128. [CrossRef]
[20] Jiang ZH, Werner DH. A Compact, Wideband Circularly Polarized Co-designed Filtering Antenna and Its Application for Wearable Devices With Low SAR. *IEEE Trans. Antennas Propag.* 2015, 63(9): 3808–3818. [CrossRef]
[21] Wu QS, Zhang X, Zhu L. Co-Design of a Wideband Circularly Polarized Filtering Patch Antenna With Three Minima in Axial Ratio Response. *IEEE Trans. Antennas Propag.* 2018, 66(10): 5022–5030. [CrossRef]
[22] Li JF, Wu DL, Zhang G, *et al.* A Left/Right-Handed Dual Circularly-Polarized Antenna With Duplexing and Filtering Performance. *IEEE Access*. 2019, 7: 35431–35437. [CrossRef]
[23] Wang W, Chen C, Wang S, Wu W. Circularly Polarized Patch Antenna With Filtering Performance Using Polarization Isolation and Dispersive Delay Line. *IEEE Antennas Wireless Propag. Lett.* 2020, 19(8): 1457–1461. [CrossRef]
[24] Tang MC, Li D, Wang Y, *et al.* Compact, Low-Profile, Linearly and Circularly Polarized Filtennas Enabled With Custom-Designed Feed-Probe Structures. *IEEE Trans. Antennas Propag.* 2020, 68(7): 5247–5256. [CrossRef]
[25] Wu QS, Zhang X, Zhu L, *et al.* Linearly and circularly polarized filtering patch antennas with enhanced gain selectivity on a single-layer substrate. *Int. J. RF Microw. Comput.-Aided Eng.* 2022, 32(3): e23029. [CrossRef]
[26] Sun GH, Wong H. Millimeter-Wave High-Gain Magneto-Electric Dipole Antenna Array With Pillbox Corporate Feed Network. *IEEE Trans. Antennas Propag.* 2021, 69(9): 5631–5639. [CrossRef]
[27] Cao QD, Yang XX, Yu F, Gao S. High Scanning Rate Millimeter-Wave Circularly Polarized CTS Leaky Wave Antenna. *IEEE Trans. Antennas Propag.* 2024, 72(7): 6087–6092. [CrossRef]
[28] Li D, Shi L, Wang J, *et al.* High-Gain Wideband Dielectric Resonator Antenna Based on Semi-Cylindrical Grooved Structure. *IEEE Trans. Circuits Syst. II Express Briefs*. 2024, 71(3): 1101–1105. [CrossRef]
[29] Ding T, Wang M, Kou A, *et al.* High-Gain Circularly Polarized Array Antenna Based on High-Order Mode ESIC for 5G Millimeter-Wave Application. *IEEE Antennas Wireless Propag. Lett.* 2024, 23(10): 3063–3067. [CrossRef]
[30] Guo QY, Yi X, Lv RC, *et al.* A High-Gain, Wideband, Circularly Polarized Antenna With Multibeam Radiation for Millimeter-Wave Applications. *IEEE Trans. Antennas Propag.* 2024, 72(2): 1373–1384. [CrossRef]

[31] Sokunbi O, Attia H, Hamza A, *et al.* New Self-Isolated Wideband MIMO Antenna System for 5G mm-Wave Applications Using Slot Characteristics. *IEEE Open J. Antennas Propag.* 2023, 4: 81–90. [CrossRef]
[32] Li Q, Liao S, Yang Y, *et al.* Wideband 5G Millimeter-Wave MIMO Magnetoelectric Dipole Antenna Integrated With Partially Reflective Surfaces. *IEEE Trans. Antennas Propag.* 2024, 72(1): 445–453. [CrossRef]
[33] Zhu C, Xu G, Ren A, *et al.* A Compact Dual-Band Dual-Circularly Polarized SIW Cavity-Backed Antenna Array for Millimeter-Wave Applications. *IEEE Antennas Wireless Propag. Lett.* 2022, 21(8): 1572–1576. [CrossRef]
[34] Rajo-Iglesias E, Ferrando-Rocher M, Zaman AU. Gap Waveguide Technology for Millimeter-Wave Antenna Systems. *IEEE Commun. Mag.* 2018, 56(7): 14–20. [CrossRef]
[35] Kishk AA, Hassan AT. Design of Large Finite Array Antennas and its Feeding Network. In: *2019 IEEE Int. Conf. Comput. Electromagn. (ICCEM)*. 2019, p.1–3. [CrossRef]
[36] Li Y, Ge L, Wang J, *et al.* A Ka-Band 3-D-Printed Wideband Stepped Waveguide-Fed Magnetoelectric Dipole Antenna Array. *IEEE Trans. Antennas Propag.* 2020, 68(4): 2724–2735. [CrossRef]
[37] Wu Y, Tomura T, Hirokawa J, Zhang M. A Wideband Full-Metal Sidewall-Loaded Magnetoelectric Dipole Array Based on Combined Ridge and Groove Gap Waveguides in the Q-Band. *IEEE Trans. Antennas Propag.* 2023, 71(7): 6156–6161. [CrossRef]
[38] Luk KM, *et al.* A microfabricated low-profile wideband antenna array for terahertz communications. *Sci. Rep.* 2017, 7(4): 1268. [CrossRef]
[39] Li X, Xiao J, Qi Z, Zhu H. Broadband and High-Gain SIW-Fed Antenna Array for 5G Applications. *IEEE Access*. 2018, 6: 56282–56289. [CrossRef]
[40] Kildal PS, Alfonso E, Valero-Nogueira A, Rajo-Iglesias E. Local Metamaterial-Based Waveguides in Gaps Between Parallel Metal Plates. *IEEE Antennas Wireless Propag. Lett.* 2009, 8: 84–87. [CrossRef]
[41] Sokunbi O, Kishk A. Dual Polarized Planar Array of Metallic Magnetoelectric Dipoles. In: *2025 19th Eur. Conf. Antennas Propag. (EuCAP)*. 2025, p.1–4. [CrossRef]
[42] Zhao Y, Luk KM. Dual Circular-Polarized SIW-Fed High-Gain Scalable Antenna Array for 60 GHz Applications. *IEEE Trans. Antennas Propag.* 2018, 66(3): 1288–1298. [CrossRef]
[43] Feng B, Tu Y, Chen J, *et al.* High-performance dual circularly-polarized antenna arrays using 3D printing for 5G millimetre-wave communications. *AEU - Int. J. Electron. Commun.* 2021, 130: 153569. [CrossRef]
[44] Wu J, Cheng YJ, Wang HB, *et al.* A Wideband Dual Circularly Polarized Full-Corporate Waveguide Array Antenna Fed by Triple-Resonant Cavities. *IEEE Trans. Antennas Propag.* 2017, 65(4): 2135–2139. [CrossRef]